Earthquakes and Structures, *Vol. 7, No. 5 (2014) 753-777*
DOI: http://dx.doi.org/10.12989/eas.2014.7.5.753

Cyclic loading tests for precast concrete cantilever walls with C-type connections

Woo-Young Lim*[a] and Sung-Gul Hong[b]

Department of Architecture and Architectural Engineering, Seoul National University, 1 Gwanak-ro, Gwanak-gu, Seoul 151-742, Republic of Korea

(Received August 28, 2014, Revised September 25, 2014, Accepted October 4, 2014)

Abstract. This study investigates the behavior of precast concrete cantilever wall systems with new vertical connections under cyclic loading. C-type steel connections for PC wall systems are proposed for the transfer of bending moments between walls in the vertical direction, whereas a shear key in the center of the wall is prepared to transfer shear forces by bearing pressure. The proposed connections are assembled easily because the directions of the slots are different at the edges of the walls. Structural performance characteristics such as the strength, ductility, and failure modes of test specimens were investigated. The longitudinal reinforcing steel bars, which are connected to the C-type connections, yielded first. Ultimate deformation was terminated owing to premature failure of the connections. The strength and deformation obtained from the cross-sectional analysis were generally similar to experimental data.

Keywords: precast concrete wall; C-type connections; failure mode; strength; deformation

1. Introduction

Precast concrete (PC) elements are widely used as structural systems in many countries because of several advantages: they save time, and their cost of construction is low. In special cases, PC walls are needed at residential buildings or apartments in high and moderate earthquake zones. For this reason, the development of new vertical connections that can resist seismic loads is essential. To provide safe earthquake-resistant structures without emulating the performance of conventional cast-in-place concrete, various steel connections have occasionally been suggested as energy dissipaters or dampers.

To achieve seismic performance in earthquake zones, numerous studies on PC walls with various connections have been performed. (Rahman and Retrepo 2000, Holden 2001, Perez *et al*. 2003, Perez *et al*. 2007, Soudki *et al*. 1995a, Soudki *et al*. 1995b, Silvestri *et al*. 2011) Early studies primarily focused on how to construct PC walls and deal with connections. Rahman and Restrepo1 tested two PC walls connected by post-tensioning only and by mild steel used as an energy dissipator, and proposed general equations that determined the tendon stress after

*Corresponding author, Ph.D., E-mail: wyarch97@snu.ac.kr
[a]Ph.D., Post-doc., E-mail: wyarch97@snu.ac.kr
[b]Ph.D., Professor, E-mail: sglhong@snu.ac.kr

http://www.techno-press.org/?journal=eas&subpage=7 ISSN: 2092-7614 (Print), 2092-7622 (Online)

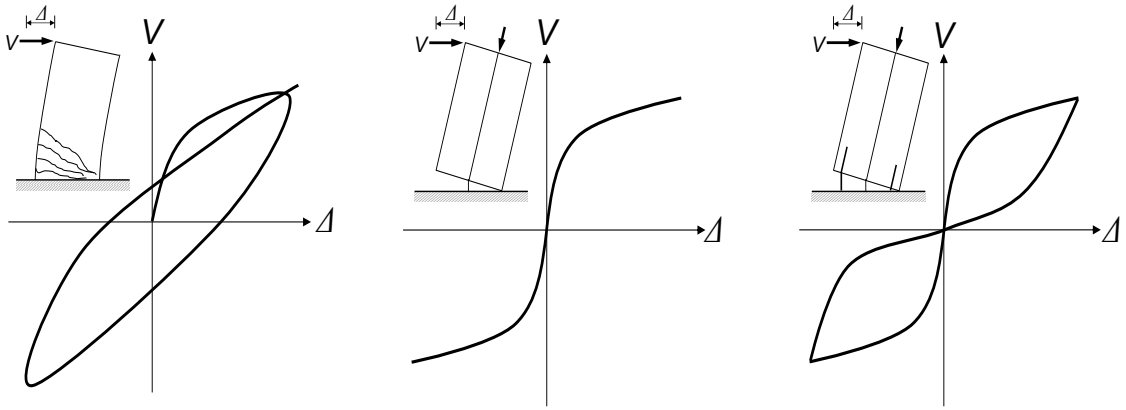

(a) Monolithic systems (b) Rocking systems (c) Hybrid systems

Fig. 1 Hysteretic response of various structural systems

decreasing the prestress. Holden (2001) performed experimental studies of PC walls using carbon fiber to minimize the crushing of concrete. Perez *et al*. (2003, 2007) conducted experimental and analytical studies on unbounded post-tensioned PC shear walls. The test walls dissipated a small amount of energy per loading cycle because only post-tensioned steel contributed to the energy dissipation. Soudki *et al*. (1995a, 1995b) conducted cyclic loading tests on PC walls of nine different connection configurations. The presence of shear keys in the horizontal connection enhanced the shear capacity in comparison with the plain surface connection.

Consequently, test specimens with unbounded post-tensioned tendons showed low energy dissipation capacity in previous studies. These systems show non-linear elastic behavior, remain damage free, and have self-centering characteristics because unbounded post-tensioned tendons alone provide moment resistance at the connection. In contrast, PC walls with additional energy dissipators display greater energy dissipation capacity than those with unbounded post-tensioned tendons (CEB FIP fib (2003)).

Fig. 1 shows the hysteretic response of various structural PC wall systems during lateral loading (CEB FIP fib (2003)). Monolithic systems such as conventional reinforced concrete (RC) wall systems designed to closely emulate the response of cast-in-place RC systems can dissipate large amounts of energy (Fig. 1(a)). Equivalent viscous damping ratios of up to 25 percent are expected for this type of construction. In contrast, fully prestressed walls have a relatively narrow hysteretic response, with a maximum equivalent viscous damping ratio of 8 percent (Fig. 1(b)). They dissipate little energy, which is expected to lead to displacement demands larger than for those systems in which energy dissipation can take place. The main source of energy dissipation is concrete crushing at the extreme ends of the connections. Equivalent viscous damping ratios for rocking frame systems are typically no more than 5 percent. Hybrid systems combine the benefits of providing a good level of energy dissipation while remaining essentially damage free (Fig. 1(c)). These systems display equivalent viscous damping ratios of up to 18 percent. Because PC walls are mainly connected by steel connections and some members are separated each other, the gap opening behavior is accompanied by additional lateral forces.

2. Research significance

This paper proposes a PC cantilever wall system with a new type of vertical connection to transfer the compressive or tensile strength for cyclic loading. Bolted connections were used for verifying the applicability of the new-type PC cantilever walls and for fast fabrication and cost reduction. Experimental studies were performed on three full-scale test specimens to evaluate the seismic performance and to verify the validity of the proposed PC walls subjected to lateral cyclic loading. The load-carrying capacity was obtained by using cross-sectional analysis and the total deformation was calculated by assuming five components of lateral displacement.

3. Development of PC walls with C-type vertical connections

The C-type vertical connections of the PC walls were proposed to transfer the bending moment between PC panels and to prevent the concrete from crushing at the edges of the PC wall panels. Fig. 2 shows the details of the proposed C-type steel connections. They consist of a pair of inner and outer steel connections. The inner connections are connected to the PC panels by using the main flexural reinforcing bars (D25) and horizontal reinforcing bar (D29) at the time of factory production. On the other hand, the outer connections are later assembled with the inner connections. The C-type connections have slots oriented in two different directions. One direction is along the wall length and the other along the wall depth (Figs. 2(a) and (b), respectively). Figs. 2(c) and 2(d) illustrate the assembling of the C-type connections with the PC panel. The flexural reinforcing bars of the PC panel are directly connected to the C-type connections. To prevent the unexpected deformation of an inner connection, a deformed horizontal reinforcing bar is used. All reinforcing bars are bolted to steel connections.

The cross-sectional size and height of the C-type connections were determined by considering the constructability, manufacturing, and costs. To determine the length, height, and thickness of the C-type connections, the following assumptions are required: 1) the size of the C-type connections is minimized; 2) the connections are maintained in elastic states until the strain of the flexural reinforcement reaches the yield strain; and 3) the reinforcing bars connected to the C-type connections or foundation do not yield or fail before the flexural reinforcing bars.

First, to determine the proper thickness of a vertical member of the outer C-type connections, cross-sectional analysis was used to obtain the depth of the neutral axis (refer to Fig. 3(a)). The longitudinal reinforcing bars and transverse reinforcements in the PC panels and C-type connections subjected to tensile and compressive forces were assumed to be negligible. To find the depth of the neutral axis, the length and width were set to L_w = 1200 mm (47.2 in.) and b_w = 150 mm (5.9 in.), respectively. The area of D25, the deformed bar used as the flexural reinforcement, is A_s = 506.7 mm^2 (0.785 in.^{2}). Cross-sectional analysis revealed that the depth of neutral axis was 28.2 mm (1.11 in.) in the final state. Thus, the thickness of the vertical steel members of the outer connections was set at 30 mm (1.18 in.). These members resist the bending moment and axial force at the edges of the walls.

The thickness of the horizontal element is obtained by the section modulus *S*, which is calculated by dividing the maximum bending moment by the allowable bending stress for the material. The slots were not considered for design the thickness of the C-type connector because the C-type connector was assumed to be a box-type connector in the early design stage. To find the

thickness of the outer connections, both ends are considered fixed and the tensile strength of the main flexural reinforcing bar is assumed to occur at the center of the connections (refer to Fig. 3(b)). The maximum moment due to the flexural reinforcing bar connected to the C-type connection is $M_{max} = (A_s f_y) l_j / 4$, where l_j represents the distance between the vertical elements with respect to center line of those elements and f_y is the yield strength of the flexural reinforcing bars (in MPa). Thus, the yield stress of the steel plate used in the outer C-type connections (in MPa) is obtained as

$$\sigma_{yp} = \frac{1.5 A_s f_y}{t_{jh}^2} \tag{1}$$

where t_{jh} is the thickness of the horizontal element of the outer connection (in mm) and A_s is the area of the flexural reinforcing bar (in mm^2).

Thus, t_{jh} is calculated as

$$t_{jh} = 1.22\sqrt{\frac{A_s f_y}{\sigma_{yp}}} \tag{2}$$

If the yield stress of the flexural reinforcing bar f_y is equal to that of the steel plate σ_{yp}, then $t_{jh} = 1.22\sqrt{A_s}$. If not, and f_y is 400 MPa (58.0 psi) and σ_{yp} is 300 MPa (43.5 psi), for example, then $t_{jh} = 1.41\sqrt{A_s}$. Thus, the thickness of the horizontal element of the proposed connection is a function of the area of the flexural reinforcing bar bolted to the connection.

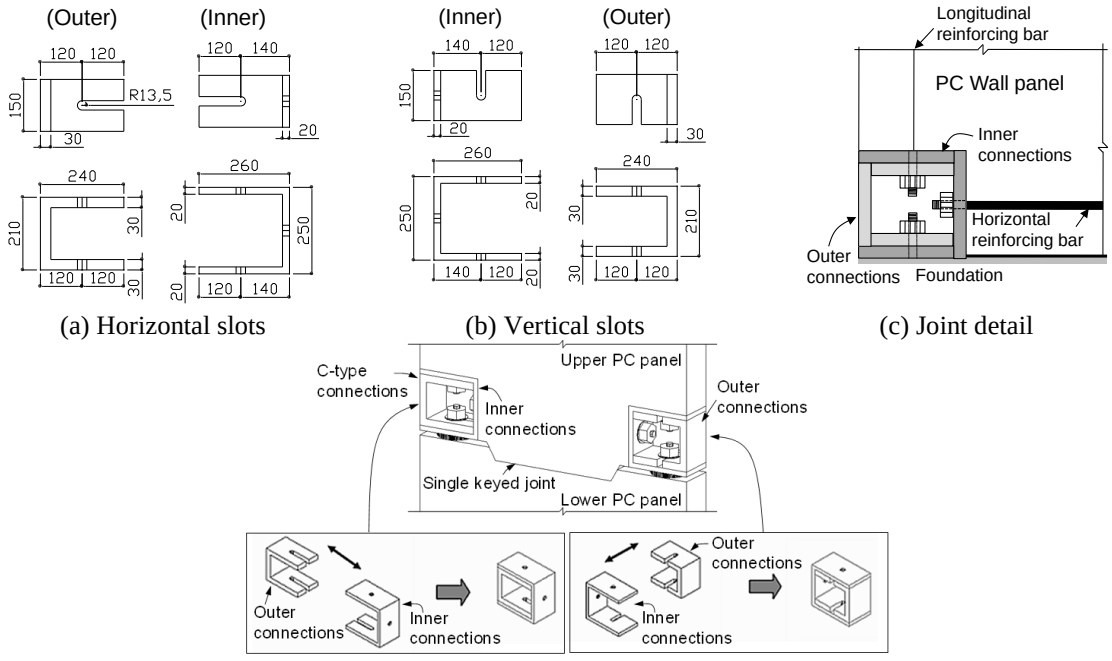

(a) Horizontal slots (b) Vertical slots (c) Joint detail

(d) Assembling of C-type connectors

Fig. 2 Details of C-type connections (Note: Dimensions in mm, 1 mm = 0.0394 in.)

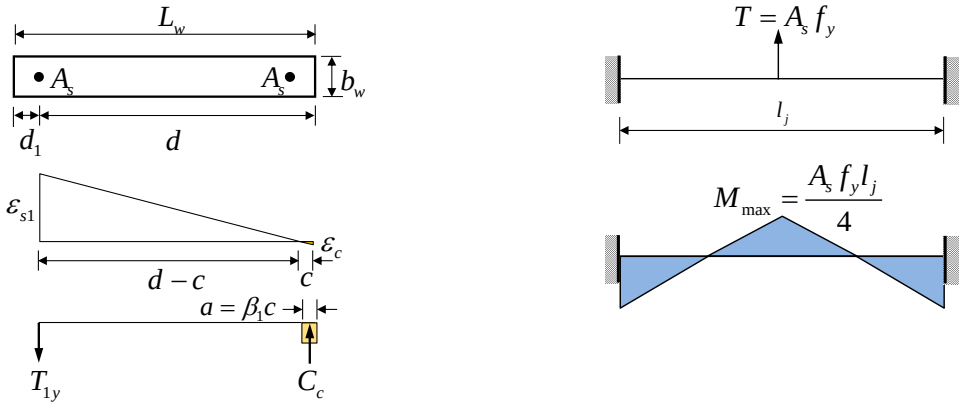

(a) Depth of neutral axis (b) Maximum moment

Fig. 3 Determination of thickness of C-type connection

Because the outer connection should be maintained in an elastic state until the main flexural reinforcing bar yields, the buckling load of the outer connection must be greater than the compressive force at the depth of the neutral axis. Because the compressive force is equal to the tensile force of the flexural reinforcing bar, the height of the outer connection (in mm) is calculated as

$$h_j < \frac{1}{k}\sqrt{\frac{\pi^2 E_{sj} I_j}{A_s f_y}} \tag{3}$$

where k is the effective length factor (k = 1), E_{sj} represents the elastic modulus of the steel plate used in the outer connections (in MPa), and I_j (= $b_w t_j^3/12$) is the moment of inertia about the weak axis for the vertical element of the outer connections (in mm^4).

However, because the inner connections were fixed, their thickness was set to 20 mm (0.8 in.) to reduce the production costs. As shown in Fig. 2, the cross-sectional dimensions of the inner and outer connections are 160 × 150 mm (6.3 × 5.9 in.) and 140 × 150 mm (5.5 × 5.9 in.), respectively. The heights of the inner and outer connections are 250 mm (9.8 in.) and 210 mm (8.3 in.), respectively.

4. Test program

Three full-scale models of two-story PC walls with C-type vertical connections were tested: a prototype (Specimen SP1), a model with diagonal reinforcing bars in the lower PC panel alone (Specimen SP2), and a model with the diagonal reinforcing bars in both upper and lower PC panels (Specimen SP3). The test specimens were designed to satisfy the requirements of ACI 318-08. Their properties and test parameters are presented in Table 1. Primary test parameters were the diagonal reinforcing bars.

The configurations and dimensions of the test specimens are shown in Fig. 4, along with details of the reinforcing bars. The height of the PC panel was h = 1200 mm (47.2 in.), and the dimensions of the rectangular cross-section were 1200 × 150 mm (47.2 × 5.9 in.). The total height

of the test specimens was 3,440 mm (135.4 in.). The net height of the PC walls measured from the surface of the foundation to the loading point was h' = 2740 mm (107.8 in.). Two D25 flexural reinforcing bars (f_y = 400 MPa [58.0 ksi]) were used to assemble the PC panels and two D32 deformed bars (f_y = 400 MPa [58.0 ksi]) were installed to connect the lower PC panel to the foundation and prevent premature failure. The D29 horizontal reinforcing bars (f_y = 400 MPa [58.0 ksi]) were placed between C-type connections at both edges of the wall.

The shear force acting on the PC panels is transferred by the shear keys and dowel action of the flexural reinforcing bars (D25) bolted to the steel connections. Fig. 4(e) shows the details of a single keyed joint, which was designed in accordance with ACI 318-08. The lengths l_{s1} and l_{s2} of the shear key are 600 mm (23.6 in) and 520 mm (20.5 in), respectively. The angle α with respect to the height of the shear key is 38.7°. To prevent premature failure of the keyed joint, twelve D10 deformed bars were installed around the C-type connections. The bearing strength of the keyed joint is obtained from the equation $V_b = 0.85 A_{vs} f_c'$, where A_{vs} is the shearing area of the keyed joint. Thus the bearing strength of the keyed joint is 255 kN (57.3 kips).

Table 1 Properties of test specimens

Specimens	SP1	SP2	SP3
Dimensions, $L_w \times h_w$ (mm×mm)	1200×1200	1200×1200	1200×1200
Total height, H_w(mm)	3440	3440	3440
Net height, H_w'(mm)	2440	2440	2440
Concrete strength, f_c'(MPa)	44.1	46.4	45.6
Flexural reinforcing bars (ρ_f*)	2-D25 (ρ_f =0.563%)	2-D25 (ρ_f =0.563%)	2-D25 (ρ_f =0.563%)
Longitudinal re-bars (ρ_l**)	8-D10 (ρ_l=0.328%)	8-D10 (ρ_l=0.328%)	8-D10 (ρ_l=0.328%)
Hoops (ρ_h§)	D10@172 (ρ_h=0.634%)	D10@172 (ρ_h=0.634%)	D10@172 (ρ_h=0.634%)
Diagonal reinforcing bars (ρ_h§§)	Upper wall panel × Lower wall panel ×	Upper wall panel × Lower wall panel 16-D13 (ρ_d=1.165%)	Upper wall panel 16-D13 (ρ_d=1.165%) Lower wall panel 16-D13 (ρ_d=1.165%)
Moment capacity at yielding, M_{fy} (kN-m)	356,600	364,700	362,400
Predicted lateral force at yielding, V_{fy} (kN)	146.2	149.5	148.5

* Ratio of flexural reinforcing bars: $\rho_f = A_{sl} / b_w L_w$

** Ratio of longitudinal reinforcing bars: $\rho_l = A_{sl} / b_w L_w$

§ Ratio of hoops: $\rho_h = A_{sh} / b_w h_w$

§§ Ratio of diagonal reinforcing bars: $\rho_d = A_{sd} / b_w L_w$

Note: 1 mm = 0.0394 in.; 1 mm^2 = 0.00155 in.^{2}.; 1 kN = 0.225 kips; 1 kN = 145 psi.

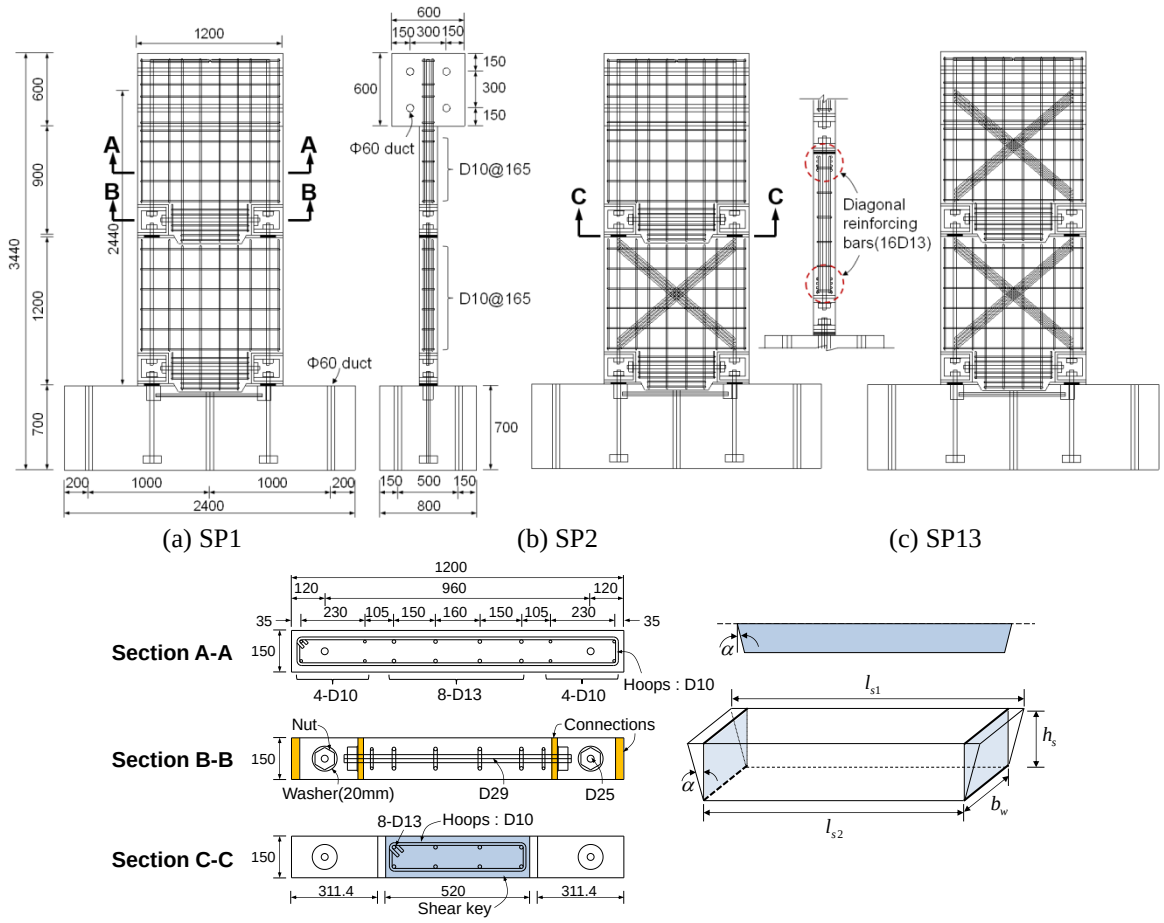

Fig. 4 Details of test specimens (Note: Dimensions in mm, 1 mm = 0.0394 in.)

Table 2 Yield and tensile strength of reinforcing bars

Size, mm		Area, mm^2	Yield strength, MPa	Tensile strength, MPa
Reinforcing bar	D25	506.7	426.6	558.2
	D29	642.4	444.2	568.5
	D32	764.2	425.0	607.5
Steel plate	T20	-	324.6	448.9
	T30	-	324.6	453.6

Note: 1 mm = 0.0394 in.; 1 mm^2 = 0.00155 $in.^2$; 1MPa = 0.145 kips

4.1 Manufacturing and assembly procedures

The test specimens were assembled as follows. First, the lower PC panel was constructed by placing the D32 reinforcing bars into the C-type connections. Next, four lateral supports were set

up to erect the PC panels vertically at the surface of the lower panel. These supports were fixed at the surface of the foundation. Subsequently, one C-type connection was fabricated with another by using nuts. One nut was used to connect the foundation to the connection, while the other nut was used to assemble the connections horizontally. Shim plates were then settled at the interface between the PC panels as needed to form a horizontal plane. An upper panel was assembled by the same method as that used to assemble the lower PC panel. After the PC walls were vertically erected, the lateral supports were removed. The horizontal joint was completed by grouting at the interfaces between PC panels.

4.2 Materials

The concrete cylinders were designed for 28-day compressive strength f_c' = 40 MPa (5.8 ksi). The compressive strengths of the concrete cylinders for SP1, SP2, and SP3 were $f_c'_{(SP1)}$ = 44.1 MPa (5.8 ksi), $f_c'_{(SP2)}$ = 46.4 MPa (6.7 ksi), and $f_c'_{(SP3)}$ = 45.6 MPa (6.6 ksi), respectively. Three 100 × 200 mm (3.9 × 7.9 in) concrete cylinders were tested according to ASTM C39/C39M-01. Concrete used in the upper and lower PC panels of each specimen was poured under the same conditions.

The average compressive strength of BCS mortar used at the interfaces between PC panels was f_c' = 50 MPa (7.3 ksi). Three 50 × 50 × 50 mm (2.0 × 2.0× 2.0 in.) cubic specimens were tested in the same manner as concrete.

Fig. 5 and Table 2 show the stress-strain relationship and strengths of the reinforcing bars as well as the steel plate, respectively. Reinforcing bars of SD400 (f_y = 400 MPa [58.0 ksi]) and steel plates of SS300 (Korean Standard, f_y = 300 MPa [43.5 ksi]) were used. The yield and tensile strengths of the flexural reinforcing bar (D25) were f_y = 426.6 MPa (61.9 ksi) and f_u = 558.2 MPa (81.0 ksi), respectively. The C-type connections were made of SS300 steel. The yield strength of the steel plate (30 mm [1.2 in] in thickness) used in the outer connections was f_{yp} = 324.6 MPa (47.1 ksi).

4.3 Test set-up

Fig. 6(a) shows the setup and instruments for testing the specimens. Lateral cyclic loading was applied to the top of the PC wall and controlled by the lateral displacement of the actuator. The target displacements for the cyclic loading were planned as drift ratios of 0.02%, 0.04%, 0.08%,

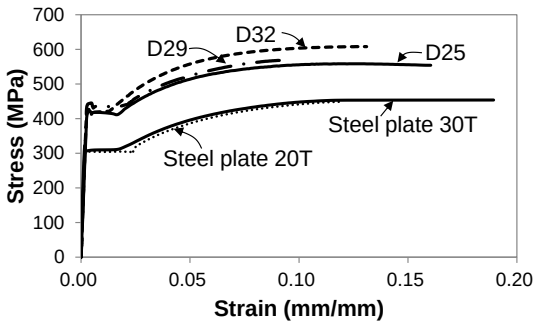

Fig. 4 Stress-strain relationship of reinforcing bars and steel plates (Notes: 1 MPa = 145 psi)

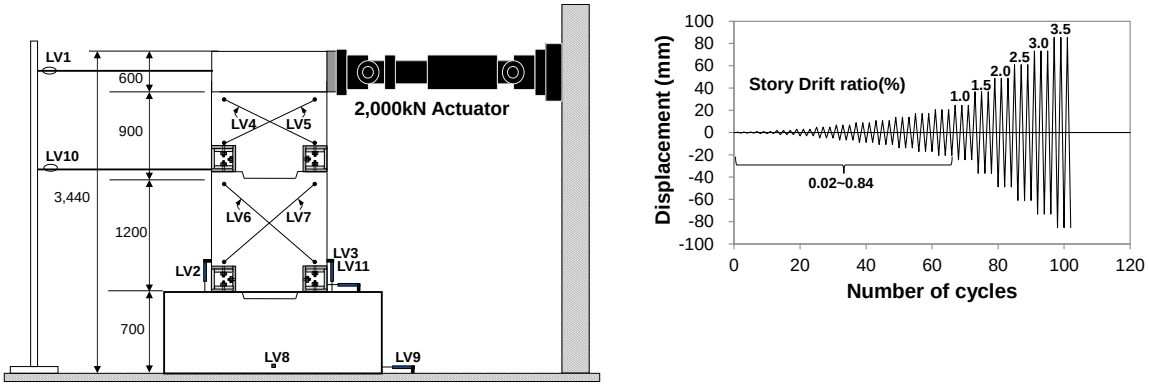

(a) SP1 (b) SP2

Fig. 6 Test setup and loading history (Notes: Dimensions in mm, 1 mm = 0.0394 in., 1 kN = 0.225 kips; LVDT is linear variable differential transformer)

0.12%, 0.20%, 0.28%, 0.36%, 0.44%, 0.56%, 0.70%, 0.84%, 1.00%, 1.50%, 2.00%, 2.50%, and 3.00%, and loading continued until ultimate failure occurred. Fig. 6(b) shows the loading schedule.

To monitor the lateral and vertical displacement during the tests, eleven linear variable differential transformers (LVDTs) were used for each specimen: LVDTs 1 and 10 for horizontal displacement at the upper PC panel; LVDTs 2 and 3 for vertical displacement at the lower PC panel; LVDTs 4, 5, 6, and 7 for diagonal deformation of the PC panel; LVDT 11 for shear slip of lower PC panel; and LVDTs 8 and 9 for unexpected displacement of foundation (Fig. 6(a)).

5. Test set-up

5.1 Lateral load-story drift ratio relationships

Figs. 7(a) to (c) show the lateral load-story drift ratio relationships. Fig. 7(d) illustrates the envelope curves of the test specimens. The lateral story drift ratio was calculated by dividing the net lateral displacement at the loading point by the net height of the PC walls. Table 3 summarizes the yield strength V_y, maximum strength V_{max}, ultimate strength V_u, yield displacement Δ_y, displacement at maximum strength Δ_{max}, ultimate displacement Δ_u, and ductility μ (Δ_u/Δ_y) of the test specimens for positive and negative loadings. The yield displacement Δ_y was defined as the point when the tensile strain of the main flexural reinforcing bar D25 reached the yield strain. The ultimate displacement Δ_u was defined as the point when the test specimen ultimately failed. The predicted load-carrying capacity V_f is also displayed in Fig. 7.

The lateral load-story drift ratio relationships of PC wall specimens were similar (Figs. 7(a) to (c)). None of the specimens showed distinct softening behavior after reaching the maximum strength. For specimen SP1, the load-carrying capacity remained constant after the maximum strength until the ultimate state. For positive loading, flexural yielding and maximum strength occurred at drift ratios of 1.0% and about 2.0%, respectively, in all specimens. In contrast, the load-carrying capacity of specimens SP2 and SP3 increased until the end of the test for positive loading. The Δ_u values of these specimens were 2.69% to 3.40%. For negative loading, flexural yielding,

Table 3 Summary of test results

Specimens	Maximum						Maximum displacement					
	Positive (+)			Negative (-)			Positive (+)			Negative (-)		
	P_{max}	Δ_{max}	Drift ratio	P_{max}	Δ_{max}	Drift ratio	P_u	Δ_u	Drift ratio	P_u	Δ_u	Drift ratio
	(kN)	(mm)	(%)	(kN)	(mm)	(%)	(kN)	(mm)	(%)	(kN)	(mm)	(%)
SP1	177.3	48.3	1.76	-146.2	-61.1	-2.23	144.8	93.1	3.40	-130.5	-73.2	-2.67
SP2	198.0	50.4	1.84	-145.1	-60.5	-2.21	203.4	73.6	2.69	-131.4	-61.1	-2.23
SP3	178.0	71.1	2.59	-136.6	-58.1	-2.12	178.0	71.1	2.59	-133.8	-63.1	-2.30

Specimens	Yielding point								P_{max}/P_y		Δ_{max}/Δ_y	
	Positive (+)				Negative (-)							
	P_y	Δ_y	Drift ratio	k_y	P_y	Δ_y	Drift ratio	k_y	Positive (+)	Negative (-)	Positive (+)	Negative (-)
	(kN)	(mm)	(%)	(kN/mm)	(kN)	(mm)	(%)	(kN/mm)				
SP1	153.0	27.1	0.99	5.65	-110.9	-25.1	-0.92	4.42	1.16	1.32	3.44	2.92
SP2	161.8	21.8	0.80	7.42	-104.4	-25.6	-0.93	4.08	1.22	1.39	3.38	2.39
SP3	148.6	32.6	1.19	4.56	-93.0	-15.9	-0.58	5.85	1.20	1.47	2.18	3.97

Notes: 1 kN = 0.225 kips; 1 mm = 0.0394 in.; 1 kN/mm = 5.71 kip/in.

maximum strength, and ultimate displacement occurred at drift ratios of -0.9%, 2.2%, and -2.4%, respectively. The measured-to-predicted yield strength ratios (V_y/V_f) for SP1, SP2, and SP3 were 1.21, 1.32, and 1.20, respectively, for positive loading. However, the peak strengths of positive and negative loadings are different each other though the specimens have symmetrical section properties. These asymmetric behaviors of all test specimens were caused by inelastic behavior of C-type connectors.

The load-carrying capacity of SP2 with diagonal reinforcing bars in the lower PC panel was greater than those of other specimens (refer to Fig. 7(d)). Only SP1 showed softening behavior after the maximum lateral load. In contrast, the load-carrying capacity for SP3 increased gradually after yielding until the end of the test. However, all specimens behaved similarly for negative loading.

The test results at the yield point, maximum load, maximum displacement, yield stiffness, and ductility of the test specimens are summarized in Table 3.

5.2 Damage patterns and failure modes

Fig. 8 shows the ultimate failure modes and damage patterns of PC walls at the end of the test. In specimen SP1, a flexural crack occurred at the left side of the lower PC panel and vertical cracks developed around the C-type connections at a drift ratio of -0.61%. Additional cracks occurred at the upper part of the lower PC panel in contact with the shear key at a drift ratio of -1.75%. Thereafter, C-type connections started to deform by increasing the lateral load. Finally, ultimate failure occurred by means of tensile failure of the flexural reinforcement D32 connecting the lower PC panel and the foundation.

For specimen SP2, the first crack was initiated at the contact surface between the shear key and the lower PC panel. At a drift ratio of 1.31%, a flexural crack started at the right side of the upper

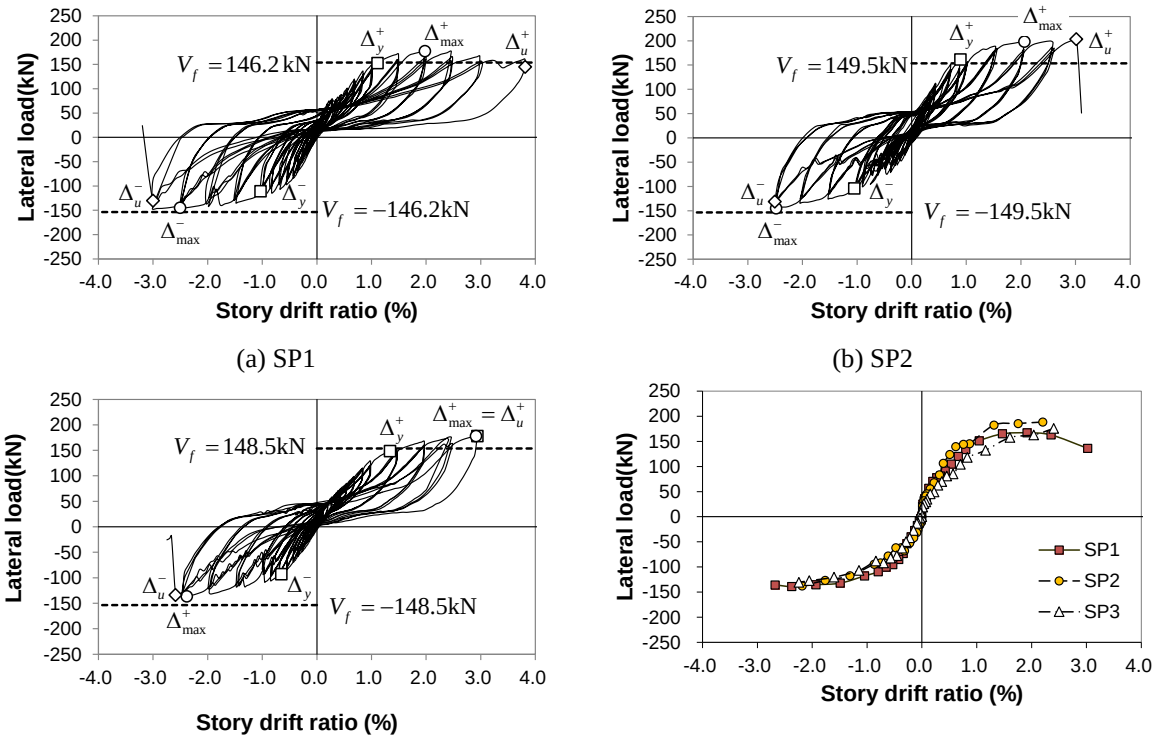

(a) SP1 (b) SP2

(c) SP3 (d) Envelop curves

Fig. 7 Lateral load-story drift ratio relationship of test specimens (Notes: 1 kN = 0.225 kips)

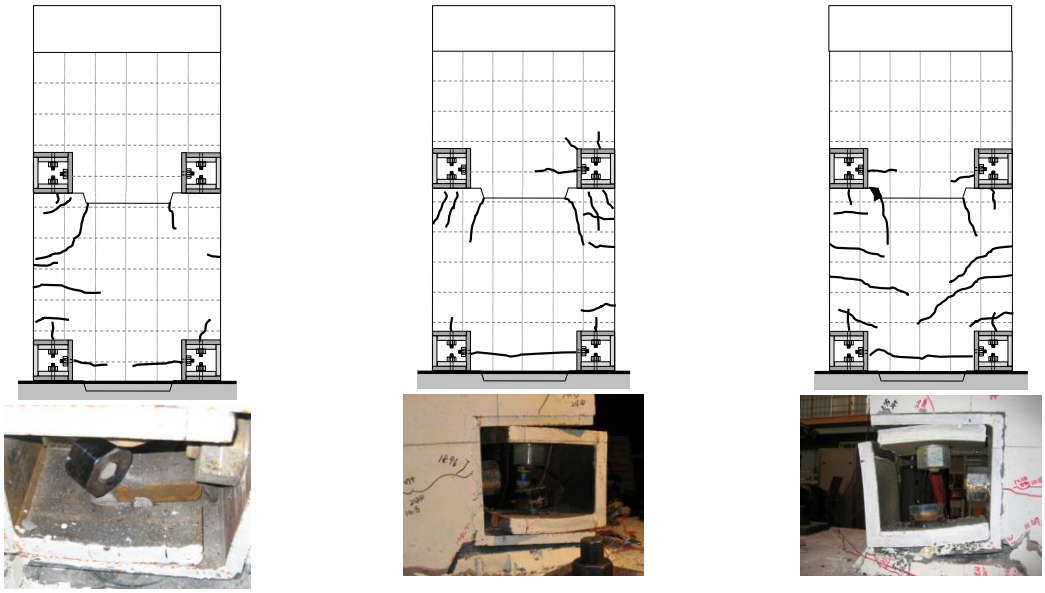

(a) SP1 (b) SP2 (c) SP3

Fig. 8 Damage patterns of test specimens

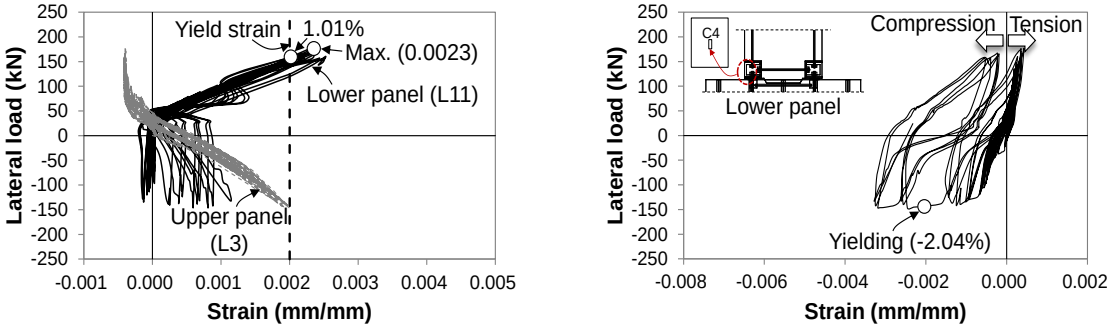

(a) SP1

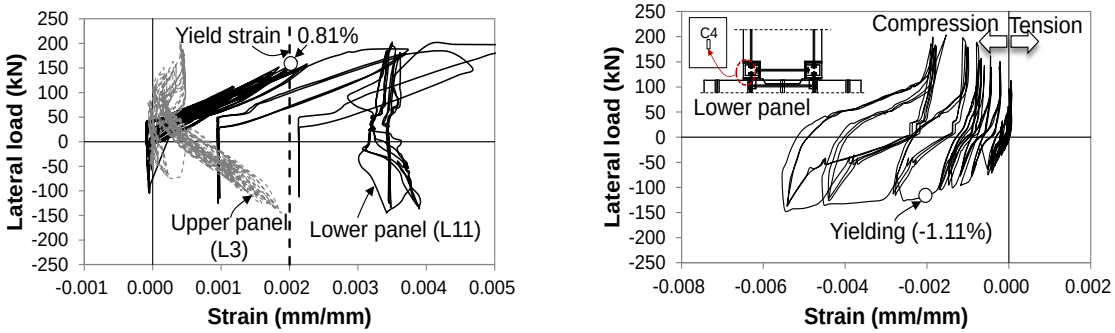

(b) SP2

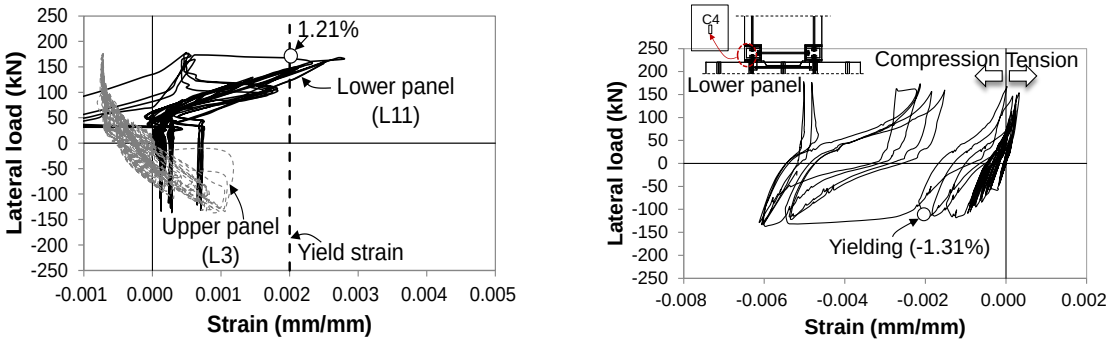

(c) SP3

Fig. 9 Measured strain of flexural reinforcing bar and C-type connections (Notes: 1 kN = 0.225 kips)

PC panel. In this specimen, the cracks were concentrated around the C-type connections of the upper PC panel. Unlike in SP1, cracks occurred at the upper PC panel, and the C-type connections remained elastic until ultimate failure. SP2 failed owing to slip of a screw connecting the C-type connections and the foundation.

In specimen SP3, the first crack was initiated at the contact surface of the shear key at -0.39%. A flexural crack occurred at the left side of the lower PC panel and a vertical crack developed around the C-type connections of the lower wall panel at -0.49%. A diagonal crack occurred in the

lower wall panel at 1.31%. However, this test was ended because of weld failure of the steel connections.

Consequently, concrete crushing did not occur at the contact surface between PC panels because the bending moment was concentrated on the C-type connections. The proposed flexural behavior was observed in all test specimens even though the PC walls were produced by laminating the two PC panels.

5.3 Strain of reinforcing bars

Fig. 9 shows the measured strain of the flexural reinforcing bars and of the vertical member of the C-type connection. Measurements of the strain gauges L11 and C4, which were attached to the flexural reinforcing bar in the lower PC panel and at the center of the vertical member of the connections, were used to verify the strain variation of the reinforcing bars and the steel plate. Comparisons between specimens revealed that the strain of the flexural reinforcing bars in the lower PC panel reached the yielding point at drift ratios of 1.01%, 0.81%, and 1.21% for SP1, SP2, and SP3, respectively. In contrast, the vertical member of the C-type connection yielded at drift ratios of -2.04%, -1.11%, and -1.31% for SP1, SP2, and SP3, respectively. These results indicate that the C-type connection maintained an elastic state until the yield point of the flexural reinforcing bars was reached.

5.4 Shear distortion

To determine the effect of the diagonal reinforcing bars, which was the primary concern, the average shear distortions at both upper and lower PC panels were evaluated. These values were obtained from the deformations measured with the LVDTs located in the lower (LVDTs 6 and 7) and upper (LVDTs 4 and 5) portions of the PC panels as

$$\gamma_{avg} = \frac{d_1\delta_1 - d_2\delta_2}{2HL} \tag{4}$$

where δ_1 represents the strain measured from LVDTs 4 and 6, and δ_2 the strain measured from LVDTs 5 and 7. d_1 and d_2 are the diagonal distances of the upper and lower PC panels. The horizontal distance between the LVDTs is L = 900 mm (35.4 in.), and the vertical distances between the LVDTs in the lower and upper PC panels, H_1 and H_2, are 900 mm (35.4 in.) and 640 mm (25.2 in.), respectively.

According to Sittipunt *et al*. (2001) and Shaingchin *et al*. (2007) reinforced concrete walls with reinforcing bars arranged in a diagonal web experienced less shear distortion in the hinging region than walls with conventional web reinforcement composed of longitudinal and transverse reinforcing bars.

Fig. 10 shows the average shear distortion of the PC wall specimens during the test. Diagonal web reinforcement also helped reduce inelastic shear distortion in the lower portion of the walls. As shown in Fig. 10, shear distortions of the upper and lower PC panels were highly similar without the diagonal reinforcing bars. The shear distortion for specimen SP3 was significantly less than that for other specimens owing to the diagonal reinforcing bars. In contrast, for specimen SP2, in which diagonal reinforcing bars were installed for the lower PC panel, test results showed that the shear distortion of the upper PC panel was greater than that of the lower PC panel.

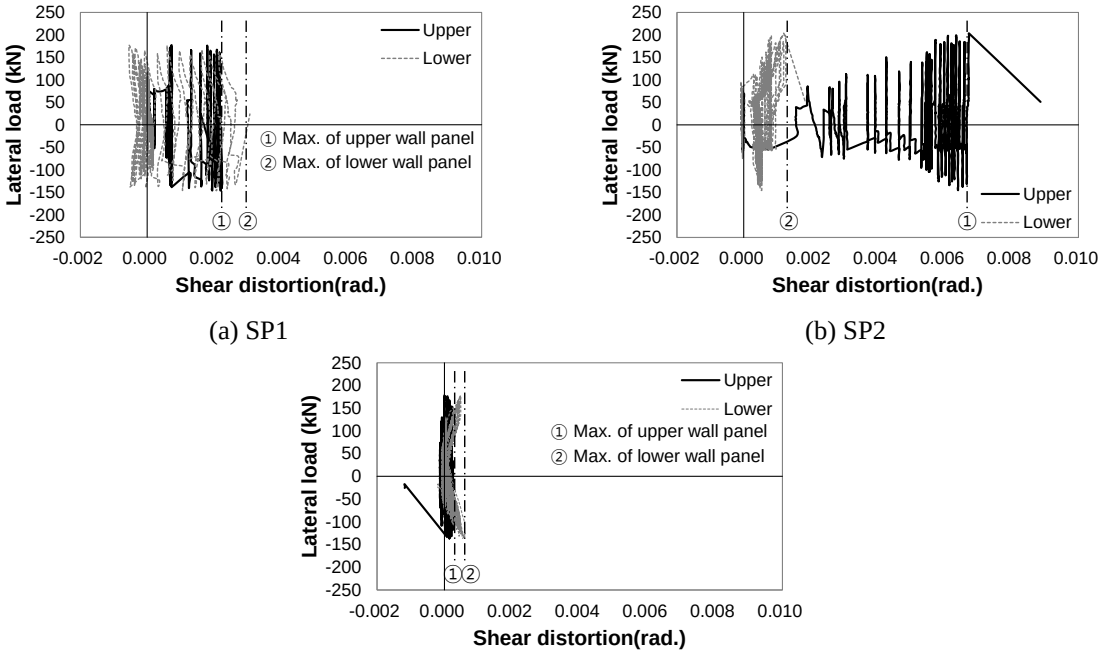

(a) SP1 (b) SP2

(c) SP3

Fig. 10 Shear distortion of test specimens (Notes: 1 kN = 0.225 kips)

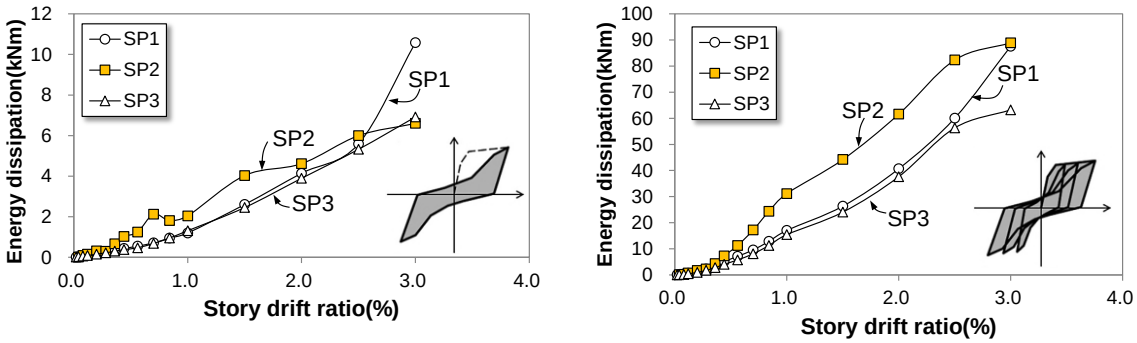

(a) Energy dissipation per load cycle (b) Cumulative energy dissipation

Fig. 11Hysteretic energy dissipation of test specimens (Notes: 1kN·m=0.738k-ft)

5.5 Energy dissipation capacity

Fig. 11 shows the hysteretic energy dissipation capacity. The energy dissipation capacity per load cycle is defined as the area enclosed by a third load cycle at a given displacement. The energy dissipation capacity of SP2 was greater than that of other specimens during cyclic loading (Fig. 11(a)). Although SP3 had the diagonal reinforcing bars in both PC panels, the energy dissipation capacity was similar to that of SP1. The ratios of the energy dissipation capacity of SP2 to that of SP1 and to that of SP3 were 1.57 (SP2 / SP1) and 1.20 (SP2 / SP3), respectively.

According to Park and Eom (2006) and Eom and Park (2010) the energy dissipation per load cycle of RC members is related to the large plastic strains of the flexural reinforcing bars. In addition, according to Sittipunt *et al*. (2001) and Shaingchin *et al*. (2007) reinforced concrete walls with diagonal web reinforcement display the ability to dissipate more energy. After yielding, the strain of the flexural reinforcing bars in the lower PC panel of SP2 was significantly greater than that of other specimens (refer to Fig. 9). Because the C-type connections of all test specimens were elastic state before yielding of main flexural reinforcement, the deformation of flexural reinforcing bars in the PC panels was important for evaluating the energy dissipation capacities.

5.6 Equivalent viscous damping ratio

The equivalent viscous damping ratio is the ratio of the area inside, to that of the rectangle circumscribing, the hysteresis loop. The area inside the hysteresis loop is equal to the energy dissipation per cycle. The equivalent viscous damping ratio (CEB FIP fib 2003) is obtained as

$$\xi_{eq} = \frac{2}{\pi}\frac{A_{loop}}{A_{rect}} \tag{5}$$

where A_{loop} represents the area enclosed by the hysteresis loop and A_{rect} is the area of the rectangle circumscribing the hysteresis loop.

Fig. 12 shows the equivalent viscous damping ratio ξ_{eq} of SP1. It also illustrates the variation of ξ_{eq} per cycle for story drift ratio. The equivalent viscous damping ratio decreased rapidly from starting point to a drift ratio of 0.5%, and reached a minimum when the flexural reinforcing bar yielded at 1.0%. Thereafter, the value increased gradually to 14.7 percent at the end of the test. These results indicate that the proposed PC wall system with C-type connections can be regarded as a hybrid system because the equivalent viscous damping ratio of the proposed system is greater than that of the fully prestressed wall system or the rocking wall system. This was mainly due to yielding of the C-type connections. Note that the energy dissipation increased after yielding because the C-type connections participated in energy dissipation after yielding of the flexural reinforcing bars.

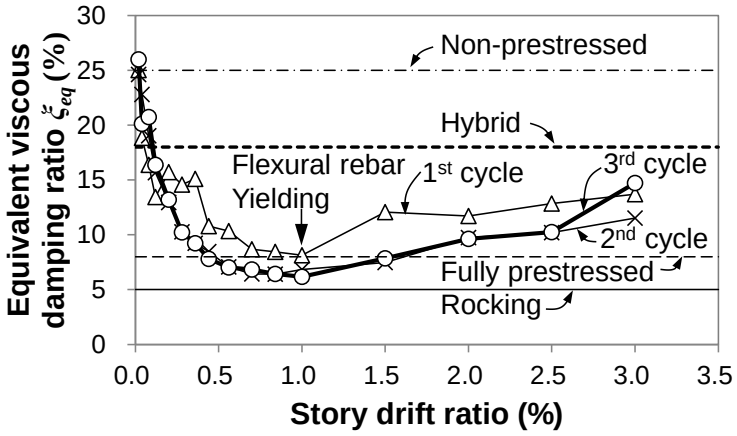

Fig. 12 Equivalent viscous damping ratio of SP1 test specimen

6. Evaluation of test results

Fig. 13(a) shows the forces on the proposed PC shear wall system with a rotation point located at a distance of *c*, which is the same as the depth of the neutral axis. At this point, the flexural reinforcing bar and the vertical elements of the C-type connection are subjected to tension. Fig. 13(b) illustrates the idealized lateral load-displacement relationship of a PC wall with C-type connections. Four limit states of the PC wall in the idealized load-displacement relationship are proposed. Originally identified by Perez *et al*. (2007) these wall limit states are presented by using the tri-linear idealized load-displacement relationship. The limit states in this study are 1) gap opening, 2) flexural yielding of the reinforcing bar, 3) maximum strength, and 4) the ultimate state of the flexural reinforcing bar. Gap opening occurs first at the connections because the C-type

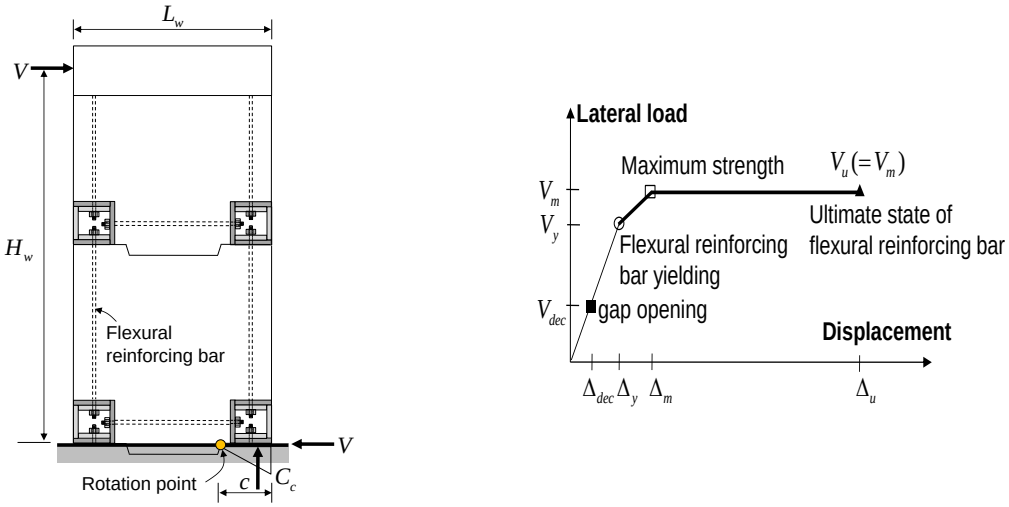

(a) Forces on the PC wall (b) Load-displacement relationship

Fig. 13 Idealized load-displacement relationship of proposed PC walls

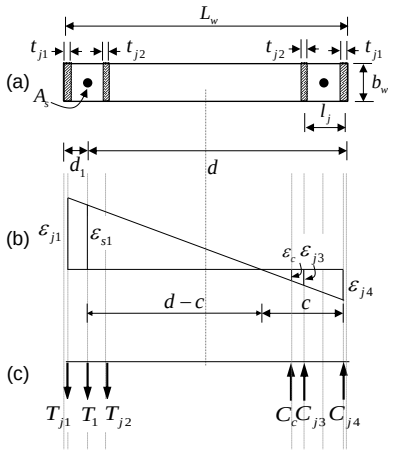

Fig. 14 Internal forces of concrete and reinforcing bars at lower PC wall panel

connections are produced without welding. Flexural yielding of the reinforcing bars is defined to occur at the point when their strains reach the yield strain obtained from material tests. The ultimate state of the proposed PC walls may be defined in terms of three potential failure mechanisms. If the strain of the compressive concrete at the depth of the neutral axis or the contact surface between shear keys reaches the ultimate strain, the lateral load will decrease after maximum load owing to the softening of concrete. However, if concrete crushing does not occur, the strain of the flexural reinforcing bar will increase continually until the tensile strain is reached, at which point the C-type connections will show elasto-plastic behavior. The lateral load may remain constant in this case. Lastly, if the compressive force acting on the C-type connections reaches the buckling load, the load-carrying capacity will decrease gradually after the peak-load.

6.1 Load-carrying capacity

The load-carrying capacity is obtained by cross-sectional analysis of the rectangular wall. Fig. 15 shows the internal forces acting on concrete, reinforcing bars, and C-type connections at lower PC wall panel. The load-carrying capacity at V_y is determined when the tensile strain ε_{s1} of the flexural reinforcing bar reaches the yield strain. To determine the depth of the neutral axis, other longitudinal reinforcing bars in the PC panels are disregarded. When ε_{s1} reaches the yield strain, the tensile force of the flexural reinforcing bar is $T_{1y} = E_s A_s \varepsilon_{s1}$; the tensile forces of the outer and inner connections are $T_{j1} = E_{sj} b_w t_{j1} \varepsilon_{s1} (d - c + l_j/2) / (d - c)$ and $T_{j2} = E_{sj} b_w t_{j2} \varepsilon_{s1} (d - c - l_j/2) / (d - c)$, respectively; the compressive force of concrete at the compression zone is $C_c = E_c \varepsilon_{s1} b_w (c - l_j) 2 / (3(d - c))$; and the compressive forces of the inner and outer connections are $C_{j1} = E_{sj} b_w t_{j1} \varepsilon_{s1} c / (d - c)$ and $C_{j2} = E_{sj} b_w t_{j2} \varepsilon_{s1} (c - l_j) / (d - c)$, respectively. E_c represents the elastic modulus of concrete.

If concrete crushing does not occur at the contact surface between the shear keys, the concrete strain of the cross-section can be considered as a linear distribution. Thus, the load-carrying capacity is obtained by $V_f = M_y / H_w$ where M_y is the flexural moment capacity at yielding and H_w is the total height of the PC wall.

6.2 Lateral displacement

The displacement of the PC structural walls consist of five components: flexural displacement Δ_f, shear displacement Δ_s, displacement due to tensile strength of reinforcement Δ_r, displacement due to internal forces at the connections Δ_j, and displacement due to gap opening Δ_{go}. Thus, the total displacement of the proposed PC wall with the C-type connections is calculated as

$$\Delta_{cal} = \Delta_f + \Delta_s + \Delta_r + \Delta_j + \Delta_{go} \tag{6}$$

To determine the components that cause total lateral displacement, the proposed PC wall is assumed to be a cantilever wall subjected to a lateral load without an axial load. Therefore, flexural displacement of the cantilever wall is estimated as

$$\Delta_f = \frac{V_f H_w^3}{3 E_c I_c} \tag{7}$$

where E_c is the elastic modulus of concrete (= $4700\sqrt{f_c'}$, in MPa) and I_c represents the moment of inertia of a cross-section of the rectangular PC wall.

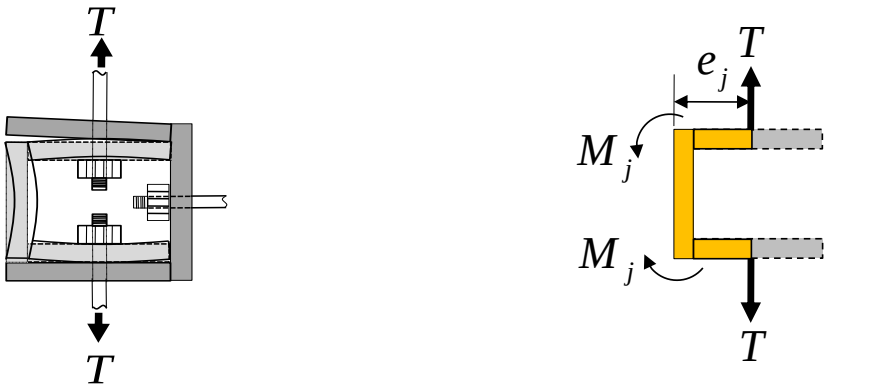

(a) Deformation of connection in tension (b) Moment at the inner connections

Fig. 15 Moment due to tensile strength of flexural reinforcing bar

Furthermore, the shear displacement is obtained as

$$\Delta_s = \frac{V_f H_w}{G_c A_e} \tag{8}$$

where G_c is the shear modulus of concrete (= E_c / 2(1+ν)), ν is Poisson's ratio, A_e is the effective shear area (= 0.4A_g) (Panneton *et al*. 2006), and A_g is the gross area of the PC wall.

When the PC wall is subjected to a lateral load, the tensile strength of the flexural reinforcing bar induces moment capacity because of the interface that exists between wall panels. Because the moment is obtained by $M_f = A_s E_s \varepsilon_{s1}(d-c)$, the displacement due to the tensile strength of the flexural reinforcing bars is calculated as

$$\Delta_r = \frac{A_s E_s \varepsilon_{s1} (d-c) H_w^2}{2 E_c I_c} \tag{9}$$

where A_s represents the area of the flexural reinforcing bar, E_s is the elastic modulus of the reinforcing bar, d is the effective depth, and c is the depth of the neutral axis.

Because additional moment capacity is applied to the outer connections (refer to Fig. 15), the vertical displacement due to this moment is given by

$$\Delta_j = \frac{A_s E_s \varepsilon_{s1} e_j H_w^2}{2 E_c I_c} \tag{10}$$

6.3 Initial stiffness

There are two common methods to determine the initial stiffness of RC or PC structural walls. The first estimates the initial stiffness from the load-displacement relationship by identifying the point at which the lateral load is 80% of the maximum as (represented by A in Fig. 16(a)). The second uses the lateral load and displacement when the strain of the flexural reinforcing bars reaches the yield strain (intersection B in Fig. 16(a)). The initial stiffness of the test specimens was determined by dividing the lateral load by the corresponding displacement at yielding for the third cycle.

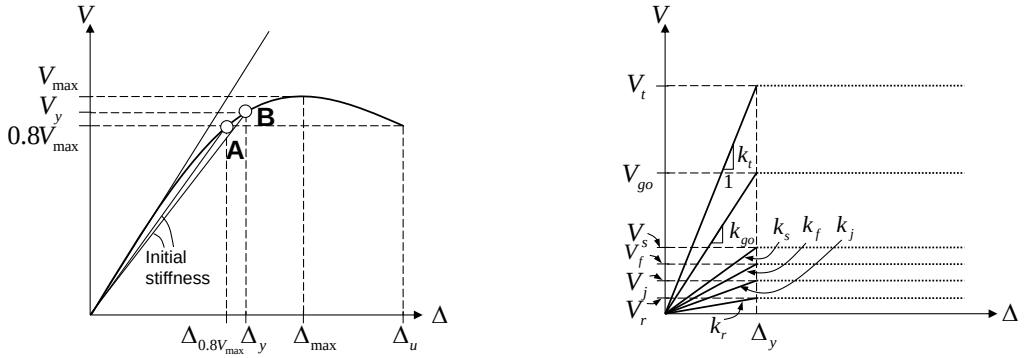

(a) Determination of initial stiffness (b) Proposed initial stiffness

Fig. 16 Determination of initial stiffness of PC walls

Fig. 16(b) shows the proposed method to estimate the theoretical initial stiffness of the PC structural walls. Because five components in all affect the initial stiffness, the theoretical initial stiffness of the proposed PC walls (Farrar *et al*. (1990)) without axial load in the elastic region is obtained as

$$k_t = \frac{1}{k_f + k_s + k_r + k_j + k_{go}} \tag{11}$$

where k_f and k_s are the stiffness for flexure (= $3E_cI_c$ / H_w^3) and shear (= G_cA_e / H_w), respectively, and k_r, k_j, and k_{go} represent the stiffness due to the elongation of the flexural reinforcing bars, moment of outer C-type connections, and gap opening. The value of k_r and k_j were calculated by using Eqs. (9) and (10).

Inserting five components into Eq. (11) and applying the effective moment of inertia $0.4I_g$ yields

$$k_t = \frac{1}{\dfrac{H_w}{E_c b_w L_w}\left[\left(\dfrac{15}{H_w}\left(jd + e_{j2}\right)+10\right)\left(\dfrac{H_w}{L_w}\right)^2 + 5.88\right] + k_{go}} \tag{12}$$

where I_g denotes the moment of inertia of gross section and $k_{go} = \dfrac{12\alpha e_{j1}e_{j2}\left(e_{j1}+h_{j1}\right)H_w}{E_{sj}b_w t_{j1}^3\left(L_w - R\right)}$.

Consequently, the predicted initial stiffness was in good agreement with the experimental data. The ratios of the expected stiffness shown in Table 3 to the predicted initial stiffness of SP1, SP2, and SP3 were 1.05, 1.37, and 0.84, respectively, for the positive loading direction. The corresponding ratios for the negative loading direction were 0.82, 0.76, and 1.08.

6.4 Gap opening

In the proposed PC wall subjected to lateral loading, gap opening occurs inevitably at the connections because the C-type connections are not welded together. To obtain the lateral

displacement due to gap opening, the vertical displacement of a C-type connection is first calculated. Fig. 17 shows the vertical displacement and deformation shape of the connections. The tensile force applied between the upper surfaces of the inner and outer connections causes the different deformation shapes. The vertical displacement δ_{vA} is defined as the size of the gap relative to that of the horizontal member of the inner connection. The angle of the gap opening is obtained from $\theta_A = \delta_{vA} / e_{j2}$.

To determine the lateral displacement due to the gap opening, the vertical displacement should first be found by means of the failure modes of the C-type connections. Thus, the inner and outer connections can be replaced with simply supported C-type frames (refer to Fig. 18).

The tensile strength of the flexural reinforcing bar is applied at a constant rate at each connection due to differences in thickness. The tensile strength T_1 is expressed by the summation of P_1 and P_2, the tensile strengths occurring at the upper and lower surfaces, respectively of each joint. However, the vertical displacements of the inner and outer connections at node a are assumed to be identical. Therefore, the following equations are satisfied.

$$\delta_{aA} = \delta_{aB} \tag{13}$$

Here, δ_{aA} and δ_{aB} represent the vertical displacements at point a. The vertical displacement is obtained by the unit load method as

$$\delta_{aA} = \int_a^b \frac{M_0 M_1}{E_{sj} I_{b1}} dx + \int_b^c \frac{M_0 M_1}{E_{sj} I_{c1}} dy + \int_d^c \frac{M_0 M_1}{E_{sj} I_{b1}} dx \tag{14}$$

where M_0 and M_1 are the moments due to the actual load and the unit load for each element of a C-type connection; and I_{b1} and I_{c1} are the moments of inertia of horizontal and vertical elements on the inner connection. Thus, the moment due to an actual load for each element is $M_{0(ab)} = M_{0(cd)} = -P_1 x$, $M_{0(bc)} = -P_1 e_{j1}$, and that due to a unit load is $M_{1(ab)} = M_{1(cd)} = -x$, $M_{1(bc)} = -e_{j1}$ for the inner connections.

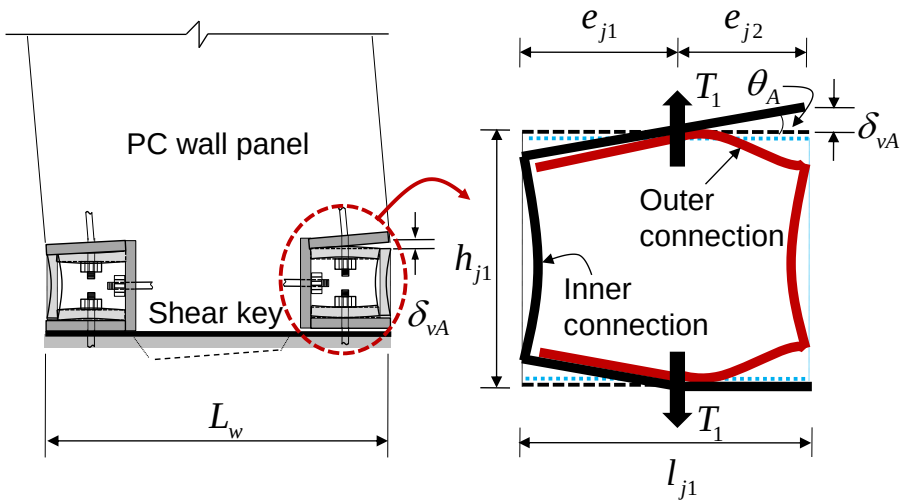

Fig. 17 Vertical displacement of C-type connections due to gap opening

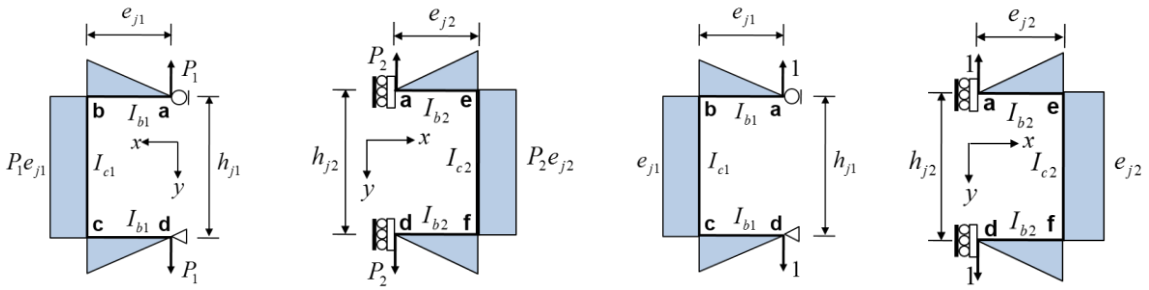

(a) M_0 of inner connection (b) M_0 of outer connection (c) M_1 of inner connection (d) M_1 of outer connection

Fig. 18 Unit load method for determining of vertical displacement

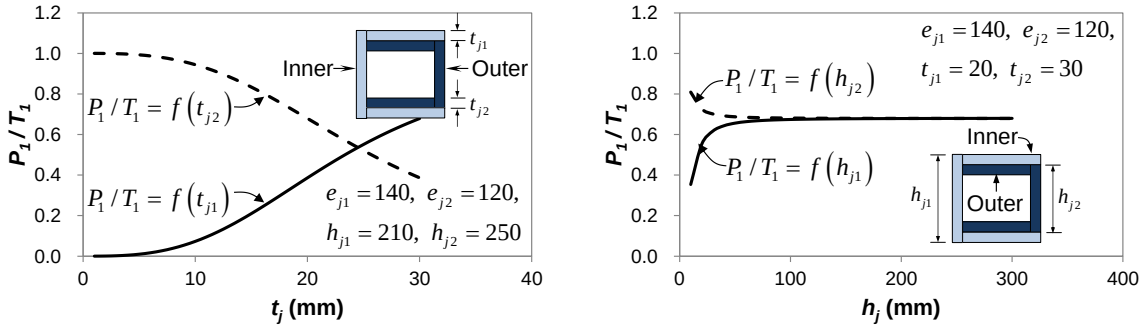

(a) Thickness of connections (b) Height of connections

Fig. 19 Ratio of tensile force P_1 to T_1 (Notes: Dimensions in mm, 1 mm = 0.0394 in.)

For the outer connections (Figs. 19(c) and (d)), their vertical displacement at node *a* can be calculated by the same method. The moment due to an actual load is obtained as $M_{0(ae)} = M_{0(fd)} = P_2x$, $M_{0(ef)} = P_2e_{j2}$, and that due to a unit load is $M_{1(ae)} = M_{1(fg)} = x$, $M_{1(ef)} = e_{j2}$. Because the length of the member *ab* is equal to that of the member *cd*, the vertical displacement δ_{aA} for the inner connections is obtained as

$$\frac{P_1}{T_1} = \frac{2e_{j2}^3 / 3I_{b2} + e_{j2}^2 h_{j2} / I_{c2}}{\left(2e_{j1}^3 / 3I_{b1} + e_{j1}^2 h_{j1} / I_{c1}\right) + \left(2e_{j2}^3 / 3I_{b2} + e_{j2}^2 h_{j2} / I_{c2}\right)} \tag{15}$$

where h_{j1} and h_{j2} are the heights of the inner and outer connections, respectively. In addition, e_{j1} and e_{j2} represent the distances between the flexural reinforcing bars and the edges of the inner and outer connections, respectively (refer to Fig. 17). Note that the tensile strength P_1, which causes the vertical displacement due to gap opening, is expressed as a function of the location of the flexural reinforcing bar (e_{j1}, e_{j2}), as well as the dimensions of the vertical and horizontal members of the C-type connection (i.e., h_{j1}, h_{j2}, I_{b1}, I_{c1}, I_{b2}, and I_{c2}).

Fig. 19 shows variation of the tensile force P_1 for primary design parameters, such as the thickness and height of the C-type connections. To compare the effect of parameters the distance e_{j1} = 140 mm (5.51 in.), e_{j2} = 120 mm (4.72 in.) were applied. As the thickness of the inner connections t_{j1} increased, the ratio of the tensile force P_1 to T_1 increased (refer to Fig. 19(a)). However, the ratio decreased as the thickness of the outer connections t_{j2} increased. In contrast, the

influence of the height of the inner and outer connections was not significant (refer to Fig. 19(b)). Substituting the actual parameters into Eq. (15), the sharing tensile forces at the inner and outer connections were $P_1 = 0.68A_sE_s\varepsilon_{s1}$ and $P_2 = 0.32A_sE_s\varepsilon_{s1}$, respectively.

The deflection angle θ_A with respect to the horizontal member *ab* is calculated by applying the virtual unit moment $M_1 = -1$ at node *a* as follows:

$$\theta_A = \frac{P_1 e_{j1}}{E_{sj}} \left(\frac{e_{j1}}{I_{b1}} + \frac{h_{j1}}{I_{c1}} \right) \tag{16}$$

Therefore, by using the deflection angle θ_A obtained by Eq. (16), the vertical displacement δ_{vA} of node *a* is determined as

$$\delta_{vA} = \theta_A e_{j2} \tag{17}$$

The total rotation angle due to gap opening θ_w is determined by the vertical displacement divided by the distance of the rotation point as

$$\theta_w = \frac{\delta_{vA}}{L_w - R} \tag{18}$$

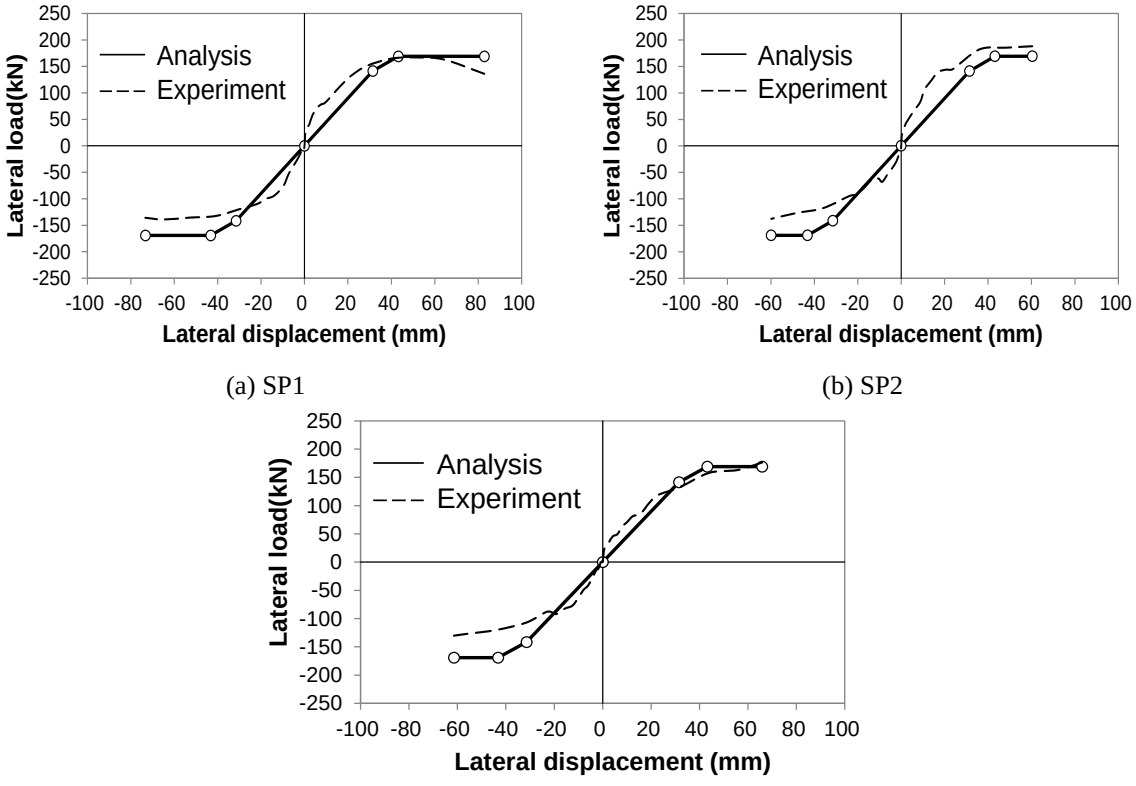

(a) SP1

(b) SP2

(c) SP3

Fig. 20 Comparison of analysis with experimental results (Notes: 1 kN = 0.225 kips)

where L_w is the total length of the PC wall, and R is the distance from the edge of the wall to rotation point (= 340 mm [13.4 in.]).

Finally, the lateral displacement due to gap opening Δ_{go} is obtained by multiplying the rotation angle θ_w by the total height H_w as

$$\Delta_{go} = \theta_w H_w \tag{19}$$

The ratio of each component to the total lateral displacement was presented to compare the contributions of the components by dividing each component by the total lateral displacement Δ_{test}. To calculate each displacement component, a compressive concrete strength of f_c' = 40 MPa was applied. Consequently, the predicted values were Δ_{fy} = 1.06 mm (0.04 in.), Δ_{sy} = 0.38 mm (0.015 in.), Δ_{ry} = 0.48 mm (0.019 in.), Δ_{jy} = 0.13 mm (0.005 in.), Δ_{goy} = 29.43 mm (1.16 in.) at yielding and were Δ_{fm} = 5.64 mm (0.22 in.), Δ_{sm} = 2.08 mm (0.08 in.), Δ_{rm} = 0.58 mm (0.023 in.), Δ_{jm} = 0.15 mm (0.006 in), and Δ_{gom} = 34.72 mm (1.37 in.) at maximum. Finally, the total lateral displacement at yielding and maximum were Δ_{caly} = 31.47 mm (1.24 in.) and Δ_{calm} = 43.18 mm (1.70 in.), respectively. Thus, the gap opening accounted for about 93.5% at yielding and 80.4% at maximum of the total displacement.

6.5 Analysis results

Fig. 20 compares the analyzed and experimental results. The predicted load-displacement relationship that resulted from the analysis was assumed to be a tri-linear relationship (refer to Fig. 14). The predicted load was obtained from the cross-sectional analysis, and the displacement Δ_{cal} was obtained by summation of five components calculated from Eq. (6). The ratio of test results to predicted displacement at yielding of test specimen SP1, SP2, and SP3 were 0.86, 0.69, and 1.04, respectively. Although the ratios of SP1 and SP2 were different between test result and prediction, predicted behavior is very similar to test results. Consequently, the analysis results agreed well with the test data, particularly for positive loading.

7. Conclusions

Three cantilever PC walls were tested for lateral loading without axial loading to evaluate seismic performance. The primary test parameters were those of the diagonal reinforcing bars. SP1 is a prototype test specimen. SP2 has diagonal reinforcing bars in the lower PC panel, whereas SP3 has them in both the lower and upper PC panels. On the basis of the test results, the findings obtained in the present study are summarized as follows:

- The diagonal reinforcing bars were shown to delay the yielding of flexural reinforcing bars. The flexural reinforcing bars of SP1 and SP3 yielded at drift ratios of 0.99% and 1.19%, respectively. However, the effect of the diagonal reinforcing bars on the behavior of the PC walls may be insignificant.
- The prototype specimen SP1 and the specimen SP2 with diagonal reinforcing bars placed in the lower PC panel failed because of the tensile failure of the longitudinal reinforcement connecting the lower PC panel and the foundation and the thread of a screw of a nut, respectively. In contrast, SP3, with diagonal reinforcement in both the upper and lower PC panels, failed due to fracture of the welded part of the C-type connections. Close attention should be paid to production of welded steel connections or to manufacturing of the thread of a screw at the flexural reinforcing

bars and the nuts.

- The ratios of the energy dissipation capacity of SP2 to that of SP1 and to that of SP3 were 1.57 (SP2/SP1) and 1.20 (SP2/SP3), respectively. The energy dissipation capacity of SP2 with diagonal reinforcing bars in the lower wall panel was greater than that of the other specimens.
- The predicted strength at yielding obtained from cross-sectional analysis was similar to the test results. For all specimens, concrete crushing in the compression zone did not occur until the end of the test. Thus, the maximum strength of the test specimen was obtained by using the measured strain of the flexural reinforcing bars in the lower wall panel.
- In a PC shear wall with unwelded dry connections, the displacement component due to gap opening accounted for more than 80% of the total displacement. The use of unwelded dry connections may offer many advantages to construct PC members in the future. Further studies on various steel connections and horizontal joints for structural integration are required.

Acknowledgments

This research was financially supported by the Ministry of Construction and Transportation of Korea (03 R&D A07-06); The authors are grateful to the authorities for their support.

References

Rahman, A.M. and Restrepo, J.I. (2000), *Earthquake Resistant Precast Concrete Buildings : Seismic Performance of Cantilever Walls Prestressd Using Unbonded Tendons*, Civil Engineering Research Report No. 2000-5, University of Canterbury, Christchurch, New Zealand.

Holden, T.J. (2001), *A Comparison of the Seismic Performance of Precast Wall Construction : Emulation an Hybrid Approaches*, Civil Engineering Research Report No. 2001-4, University of Canterbury, Christchurch, New Zealand.

Perez, F.J., Pessiki, S., Sause, R. and Lu, L.W. (2003), "Lateral load tests of unbonded post-tensioned precast concrete walls", Large Scale-Scale Structural Testing, Edited by Ma. A. Issa, Y.L. Mo, America Concrete Institute, Farmington Hills, Michigan, 161~183.

Perez, F.J., Sause, R. and Pessiki, S. (2007), "Analytical and Experimental Lateral Load Behavior of Unbonded Posttensioned Precast Concrete Walls", *J. Struct. Eng.*, **133**(11), 1531-540.

Soudki, K.A., Rizkalla, S.H. and LeBlanc, B. (1995a), "Horizontal Connections for Precast Concrete Shear Walls subjected to Cyclic Deformations. Part 1: Mild steel connections", *PCI J.*, **40**(4), 78-97.

Soudki, K.A., Rizkalla, S.H. and LeBlanc, B. (1995b), "Horizontal Connections for Precast Concrete Shear Walls subjected to Cyclic Deformations. Part 2: Prestressed connections", *PCI J.*, **40**(5), 82-96.

Silvestri, S., Gasparini, G. and Trombetti, T. (2011), "Seismic design of a precast R.C. structure equipped with viscous dampers", *Earthq. Struct.*, **2**(3), 297-321.

CEB-FIP fib (2003), "Seismic design of precast concrete building structures: State-of-art report", Task Group 7.3 Fédération internationale du béton, 254.

ACI 318-08 (2008), *Building Code Requirements for Structural Concrete and Commentary*, ACI Committee 318, American Concrete Institute, 473.

ASTM (2001), "Standard test method for compressive strength of cylindrical concrete specimens", C39/C39M-01, West Conshohocken, PA.

Sittipunt, C., Wood, S.L., Lukkunaprasit, P. and Pattararattanakul, P. (2001) "Cyclic behavior of reinforced concrete structural walls with diagonal web reinforcement", *ACI Struct. J.*, **98**(4), 554-562.

Shaingchin, S., Lukkunaprasit, P. and Wood, S.L. (2007), "Influence of diagonal web reinforcement on cyclic behaivor of structural walls", *Eng*. *Struct*., **29**(4), 498-510.

Park, H.G. and Eom, T.S. (2006), "A simplified method for estimating the amount of energy dissipated by flexure-dominated reinforced concrete members for moderate cyclic deformations", *Earthq*. *Spectra*, **22**(3), 1351-1363.

Eom, T.S. and Park, H.G. (2010), "Evaluation of energy dissipation of slender reinforced concrete members and Its applications", *Eng*. *Struct*., **32**(9), 2884-2893.

Panneton, M., Leger, P. and Tremblay, R. (2006), "Inelastic analysis of a reinforced concrete shear wall building according to the national building code of canada 2005", *Can*. *J*.*Civil Eng*., 854-871.

Farrar, C.R. and Baker, W.E. (1990), "Stiffness and hysteretic energy loss of a reinforced-concrete shear wall", *Experim*. *Mech*., **30**(1), 95-100.